SCIENTIFIC REPORTS
nature research

OPEN

Realizing High Thermoelectric Performance at Ambient Temperature by Ternary Alloying in Polycrystalline $Si_{1-x-y}Ge_xSn_y$ Thin Films with Boron Ion Implantation

Received: 26 March 2019
Accepted: 5 September 2019
Published online: 04 October 2019

Ying Peng[1,2], Lei Miao[2], Jie Gao[2], Chengyan Liu[2], Masashi Kurosawa[1,3,4], Osamu Nakatsuka[1,5] & Shigeaki Zaima[6]

The interest in thermoelectrics (TE) for an electrical output power by converting any kind of heat has flourished in recent years, but questions about the efficiency at the ambient temperature and safety remain unanswered. With the possibility of integration in the technology of semiconductors based on silicon, highly harvested power density, abundant on earth, nontoxicity, and cost-efficiency, $Si_{1-x-y}Ge_xSn_y$ ternary alloy film has been investigated to highlight its efficiency through ion implantation and high-temperature rapid thermal annealing (RTA) process. Significant improvement of the ambient-temperature TE performance has been achieved in a boron-implanted $Si_{0.864}Ge_{0.108}Sn_{0.028}$ thin film after a short time RTA process at 1100 °C for 15 seconds, the power factor achieves to 11.3 $\mu Wcm^{-1} K^{-2}$ at room temperature. The introduction of Sn into $Si_{1-x}Ge_x$ dose not only significantly improve the conductivity of $Si_{1-x}Ge_x$ thermoelectric materials but also achieves a relatively high Seebeck coefficient at room temperature. This work manifests emerging opportunities for modulation Si integration thermoelectrics as wearable devices charger by body temperature.

Taking advantage of the Seebeck effect, the thermoelectric generator (TEG) as a type of energy harvester can deliver an electrical output power by converting a heat stream flowing there through. Shrinking and integrating TEGs present exceptional advantages like simplicity, size and power scalability, adaptability to different temperature ranges and a long-time stability facilitated by the absence of mobile parts[1]. The wearable TEGs is, a logical fit to harvest power from the thermal energy of body and use the harvested power to operate portable electrical systems[2]. e.g. mobile and wearable electronic devices, reject the batteries replacement process forever.

Recently, ambient thermoelectrics have been developed very quickly, such as poly(3,4-ethylenedioxythiophene)-poly(styrenesulfonate) (PEDOT:PSS)[3–5] and its composites with tellurium nanowires[6,7] carbon nanotubes (CNTs)[8], or metal-containing conducting polymer, poly[K_x(Ni-ett)], which delivered an equally high power factor (PF) of up to 4.53 $\mu W\ cm^{-1}\ K^{-2}$ and an encouraging zT value of 0.3[9]. etc. However, ambient thermoelectricity still struggles with the lack of low-cost, abundant, and environmentally friendly materials. With the possibility of integration in the technology of semiconductors based on silicon (Si) electronics, high harvested power density, abundant on earth, nontoxicity, and cost-efficiency, silicon germanium ($Si_{1-x}Ge_x$) alloy has attracted significant attention among other thermoelectric materials[10,11]. However, despite its high power factor, Si is inefficient at room temperature. The efficiency of TEGs for wearable using depends on the properties of thermoelectric

[1]Department of Materials Physics, Graduate School of Engineering, Nagoya University, Nagoya, 464-8603, Japan. [2]Guangxi Key Laboratory of Information Material, School of Material Science and Engineering, Guilin University of Electronic Technology, Guilin, 541004, China. [3]PRESTO, Japan Science and Technology Agency, 4-1-8, Honcho, Kawaguchi, Saitama, 332-0012, Japan. [4]Institute for Advanced Research, Nagoya University, Nagoya, 464-8601, Japan. [5]Institute of Materials and Systems for Sustainability, Nagoya University, Nagoya, 464-8601, Japan. [6]Institutes of Innovation for Future Society, Nagoya University, Nagoya, 464-8601, Japan. Correspondence and requests for materials should be addressed to M.K. (email: kurosawa@nagoya-u.jp) or O.N. (email: nakatsuka@nagoya-u.jp)

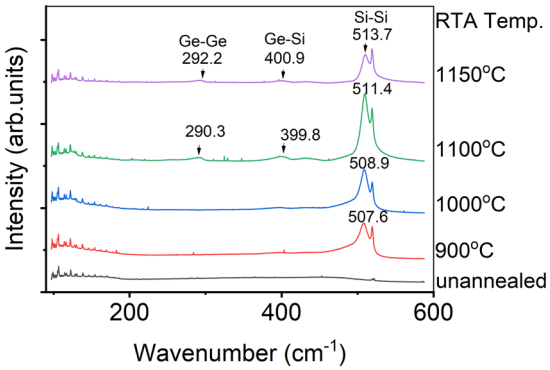

Figure 1. Raman spectra of the $Si_{1-x-y}Ge_xSn_y$ samples after 15 seconds-RTA.

materials at room temperature. The biggest challenge for Si based wearable TEGs is to achieve a high thermoelectric performance at an ambient temperature instead of its high temperature TE applications.

Three material properties, Seebeck coefficient S, conductivity σ, and thermal conductivity κ, are vital to the thermoelectric generation[12], and $zT = S^2\sigma T/\kappa$ is employed to evaluate the thermoelectric performance of materials,where T is the absolute temperature. The power factor ($PF = S^2\sigma$) could be largely enhanced through the optimization of carrier concentration, convergence of electronic bands[13], energy filtering effect[14], and quantum confinement[15], etc.

Nonetheless, polycrystalline $Si_{1-x-y}Ge_xSn_y$ ternary alloy is chosen over other materials, such as poly-Si, poly-$Si_{1-x}Ge_x$, and Bi_2Te_3 compounds. We previously reported the improvement of the thermoelectric performance of $Ge_{1-x}Sn_x$ with Sn incorporating into Ge[16]. In this study, we expect that Sn incorporation into $Si_{1-x}Ge_x$ and boron (B) ion implantation have been taken as innovated ways to improve ambient Seebeck coefficient and electrical conductivity simultaneously. A theoretical prediction for the thermal conductivity of $Si_{1-x-y}Ge_xSn_y$ ternary alloy has been recently reported[17], however there are few experimental study of $Si_{1-x-y}Ge_xSn_y$ thin films for investigating thermoelectric properties. Moreover, the recent interest in Sn by its possibility to reach direct band gaps[18,19], which is possible to improve the electrical conductivity materials and reduce the thermal conductivity of $Si_{1-x}Ge_x$ thin films.

Hence, in this study, polycrystalline $Si_{1-x-y}Ge_xSn_y$ ternary alloy film on insulator has been investigated to highlight its efficiency through ion implantation and high-temperature rapid thermal annealing (RTA) process. Significant improvement of the TE performance has been realized in B-implanted $Si_{0.864}Ge_{0.108}Sn_{0.028}$ thin films after a short time RTA at 1100 °C for 15 seconds, the power factor is 11.3 $\mu Wcm^{-1} K^{-2}$ at room temperature. The introduction of Sn into $Si_{1-x}Ge_x$ not only significantly improves the conductivity of $Si_{1-x}Ge_x$ thermoelectric materials at room temperature but also provides a relatively high Seebeck coefficient possible by the increasing of grain size due to the liquid Sn in high temperature accelerating the growth of $Si_{1-x}Ge_x$ grain[20]. The method of ion-implantation and grain size increasing achieved by Sn doping into polycrystalline $Si_{1-x}Ge_x$ thin films, and our design not only boosts the thermoelectric application of $Si_{1-x}Ge_x$-based materials but also enables a synergetic strategy for designing thermoelectric materials with high thermoelectric performance.

Results and Discussion

Figure 1 shows the Raman spectra of the samples annealed at different temperatures for 15 seconds. The Raman spectrum of the ternary $Si_{1-x-y}Ge_xSn_y$ films looks similar to the Raman spectrum of binary $Si_{1-x}Ge_x$ with comparable Si contents[21,22], and the four dominant peaks assigned to Ge-Ge, Si-Ge, and Si-Si modes from $Si_{1-x-y}Ge_xSn_y$ alloys and the Si substrate which are approximately observed at 290, 400, 510, and 520 cm^{-1} respectively. However, four visible peaks of ternary $Si_{1-x-y}Ge_xSn_y$ alloy is observed in the sample only over 1100 °C-annealing as shown in Fig. 1. One can see a clear trend that the peak intensity increases with the RTA temperature, but the 1100 °C-RTA sample is an inflection point, the peak intensity becomes weak instead in the 1150 °C-RTA sample which indicates that polycrystalline $Si_{1-x-y}Ge_xSn_y$ thin film be synthesized well only at an appropriately high RTA condition at 1100 °C for 15 seconds in our samples. The peak shift of Si-Si and Ge-Ge peaks to a higher wavenumber indicate the Sn content in ternary compounds decreases with the increasing RTA temperature[23]. The results of laser Raman measurements indicated that suitable annealing parameter not only promotes the polycrystallization of $Si_{1-x-y}Ge_xSn_y$ ternary alloy but also affects the Sn precipitation.

In order to reveal the effect of the introduction of Sn on the ternary compound's crystallization, we also prepared $Si_{0.889}Ge_{0.111}$ binary alloy samples with the same B dose for comparison. Figure 2(a,b) shows the XRD profiles of $Si_{1-x-y}Ge_xSn_y$ and $Si_{0.889}Ge_{0.111}$ samples, respectively, annealed for 15 seconds at different temperatures. Figure 2(b) show that the three higher intensity peaks locate at 2θ approximate 28.3, 47.2 and 56.0 degree which are similarly attributed to $Si_{1-x}Ge_x$ Bragg reflections of 111, 220, and 311, respectively[24]. Whereas, in Fig. 2(a) with the increase of annealing temperature, the peak intensity of $Si_{1-x-y}Ge_xSn_y$ increased more distinctly compared to $Si_{0.889}Ge_{0.111}$ samples, especially when the annealing temperature exceeds 1000 °C. Meantime, the diffraction peak related to β-Sn phase appears, especially obvious in the 1150 °C-annealed sample which means that even a short time of 15 seconds and high temperature annealing can cause part of the Sn precipitation.

The cross-sectional grain size (g) of the film could be calculated from the full width at half maximum (FWHM) of the diffraction peaks of the 111 Bragg reflection using the Scherrer formula $g = K\lambda/B\cos\theta$[25] and the lattice

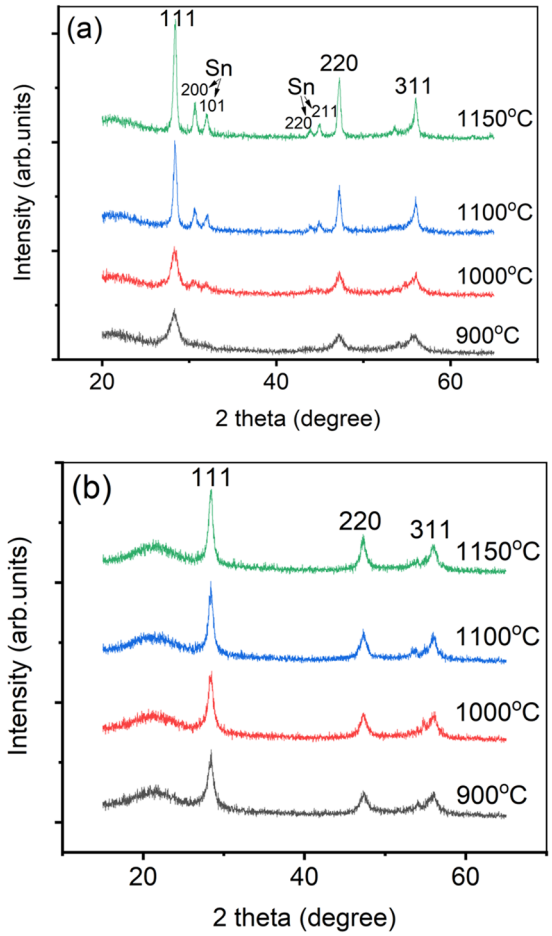

Figure 2. XRD profiles of (**a**) $Si_{1-x-y}Ge_xSn_y$ and (**b**) $Si_{0.889}Ge_{0.111}$ samples after 15 seconds-RTA.

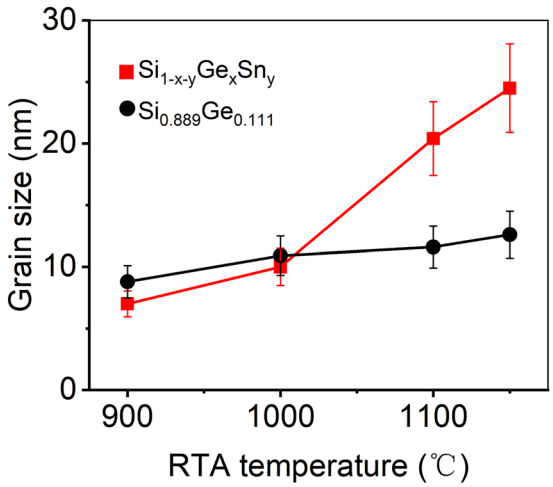

Figure 3. The RTA temperature dependence of the grain size for samples after 15 seconds-RTA.

spacing d_{111} can be calculated by the Bragg's law $2dsin\theta = \lambda$[26]. Here λ is the wavelength (0.154 nm) of Cu $K_{\alpha 1}$, θ is the angle satisfying Bragg's law, and B is the corrected FWHM in radian, $K \approx 0.9$. Generally, the crystallinity of polycrystalline $Si_{1-x}Ge_x$ thin film has been improved with the increase of annealing temperature[27].

Figure 3 shows the grain sizes in both $Si_{1-x-y}Ge_xSn_y$ and $Si_{0.889}Ge_{0.111}$ thin films increase with increasing annealing temperature, but the grain sizes increase in $Si_{1-x-y}Ge_xSn_y$ samples increases obviously faster than those of $Si_{0.889}Ge_{0.111}$ samples specifically when the RTA temperature over 1000 °C. Without doubt the 15 seconds shorter

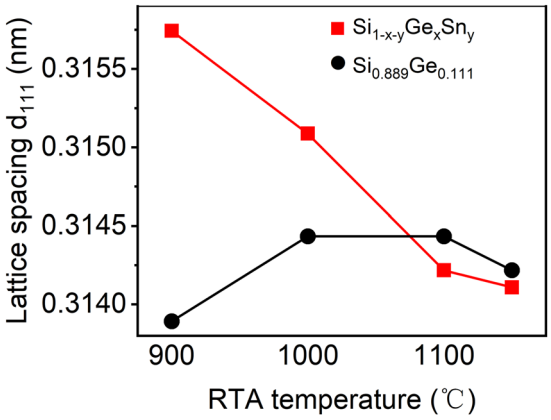

Figure 4. The RTA temperature dependence of the lattice distance for samples after 15 seconds-RTA.

RTA process led to small crystallites diameters as well, as mentioned in the first section, the precipitated liquid Sn could prominently increase the grain size of $Si_{1-x-y}Ge_xSn_y$ in 1100–1150 °C range[20], and perhaps the existence of high concentration boron atoms also attribute to rapid crystallite precipitation[28].

Figure 4 shows the lattice distance d_{111} of ternary and binary alloy thin films as a function of the annealing temperature. The lattice distance was estimated from the diffraction peak position of the Bragg reflection. Comparison the tendency of $Si_{1-x-y}Ge_xSn_y$ and $Si_{0.889}Ge_{0.111}$, the turning point is 1000 °C. When the RTA temperature locates under 1000 °C, the evident smaller d_{111} lattice spacing of $Si_{0.889}Ge_{0.111}$ confirms the formation of ternary $Si_{1-x-y}Ge_xSn_y$ in Sn doping $Si_{1-x}Ge_x$ film, while when RTA temperature exceeds 1000 °C, the rapidly decline of lattice spacing d_{111} for $Si_{1-x-y}Ge_xSn_y$ samples suggests precipitation of Sn from ternary alloy.

Figure 5(a–c) show the surface SEM images and electron dispersive spectroscopy (EDS) analyses of $Si_{1-x-y}Ge_xSn_y$ and $Si_{0.889}Ge_{0.111}$ samples after RTA at various temperatures for 15 seconds, respectively. In Fig. 5(a), the uniform grain sizes and smooth surface are observed for 900 and 1000 °C -RTA samples. While non uniform metal Sn with average particles sizes of around 40 nm are clearly seen for 1100 °C post-annealing sample in $Si_{1-x-y}Ge_xSn_y$. The size of Sn particles increases to 60 nm for 1150 °C post-annealing sample. In Fig. 5(b) for a comparison, in $Si_{0.889}Ge_{0.111}$ samples, there are no any precipitation observed on the surface except the grain size increased from about 7 to 10 nm. This result agrees well with those of Raman and XRD. In Fig. 5(c), in order to eliminate the influence of Si and O_2 content from the Si/SiO_2 substrate, the changes of Ge and Sn ratios can be analyzed by EDS at each point, the ratios for Ge and Sn at points 1 and 2 of bright regions are estimated to be 0.83%, and 1.2%, respectively, while the ratio of Sn at point 3 of a darker region is just approximate 0.2%, which further verify that the Sn precipitates out when the annealing temperature exceeds 1100 °C, and the size of Sn particles increases rapidly with the annealing temperature.

Figure 6(a,b) show the Hall mobility, carrier concentration, and conductivity of samples annealed at different temperatures for $Si_{1-x-y}Ge_xSn_y$ and $Si_{0.889}Ge_{0.111,}$ respectively. The conductivity of $Si_{1-x-y}Ge_xSn_y$ samples increases faster than that of $Si_{0.889}Ge_{0.111}$ samples and when the annealing temperature over 1100 °C the mobility of $Si_{1-x-y}Ge_xSn_y$ samples are twice as large as corresponding $Si_{0.889}Ge_{0.111}$ samples. Moreover, the improved annealing temperature under conditions of carrier concentration of $10^{20}\,cm^{-3}$ order of magnitude which is contrary to the rule that the mobility decreases with the increase of carrier concentration[29] as shown in Fig. 6(a,b), which attributing to suitable grain sizes and boundaries increase influence with heavy B doping[30,31]. After checking the carrier concentration data, one can find at least 900 °C-annealing is necessary for activation the implanted B ions[29,32] for heavily doped samples of more than $10^{15}\,cm^{-2}$ dosage, furthermore annealing of more than 1000 °C, even if only for 15 seconds, can activate most of implanted B atoms, and even at the temperature of 1150 °C, almost all the implanted B atoms are activated which leading the measured Hall carrier concentration value is larger than the designed value $1.8 \times 10^{20}\,cm^{-3}$.

Figure 7(a,b) show the thermoelectric performance of $Si_{1-x-y}Ge_xSn_y$ and $Si_{0.889}Ge_{0.111}$ samples with same B dose. In Fig. 7(a), the conductivity of $Si_{1-x-y}Ge_xSn_y$ and $Si_{0.889}Ge_{0.111}$ samples improves with the increase of RTA temperatures, obviously the conductivity of $Si_{1-x-y}Ge_xSn_y$ increases faster than that of $Si_{0.889}Ge_{0.111}$ samples. One can find that after 1150 °C-RTA treated for 15 seconds, the maximum conductivity 175 S/cm of $Si_{0.889}Ge_{0.111}$ sample is less than a third of corresponding 568 S/cm of $Si_{1-x-y}Ge_xSn_y$ sample which is attributed to the high activation rate of implanted B atoms, the better crystallinity and larger grain size caused by Sn introduction. The increased carrier mobility revealed by Hall measurements is in good agreement with electrical conductivity results. All of the samples measured at room temperature showed positive Seebeck coefficients, mean the p-type semiconductors, which match the B implantation procedure well. Generally, with the higher carrier concentration over $10^{20}\,cm^{-3}$, improving carrier mobility is the most effective way to increase both electrical conductivity and Seebeck coefficient[33–35]. Therefore, the Seebeck coefficient and conductivity of $Si_{1-x-y}Ge_xSn_y$ samples are higher than the corresponding $Si_{0.889}Ge_{0.111}$ samples. And the maximum Seebeck coefficient of $Si_{1-x-y}Ge_xSn_y$ samples is 165 μV/K which is 1.8 times higher than a $Si_{0.75}Ge_{0.25}$ microcrystalline film doped with boron at $1.6 \times 10^{20}\,cm^{-3}$, confirming the inverse dependence of Seebeck coefficient on carrier concentration[36]. Naturally, the maximum power factor $S^2\sigma$ value is calculated as 11.3 $\mu W cm^{-1}\,K^{-2}$,which is about 1.5 times higher than the bulk $Si_{80}Ge_{20}$[37,38]. In Fig. 7(b),

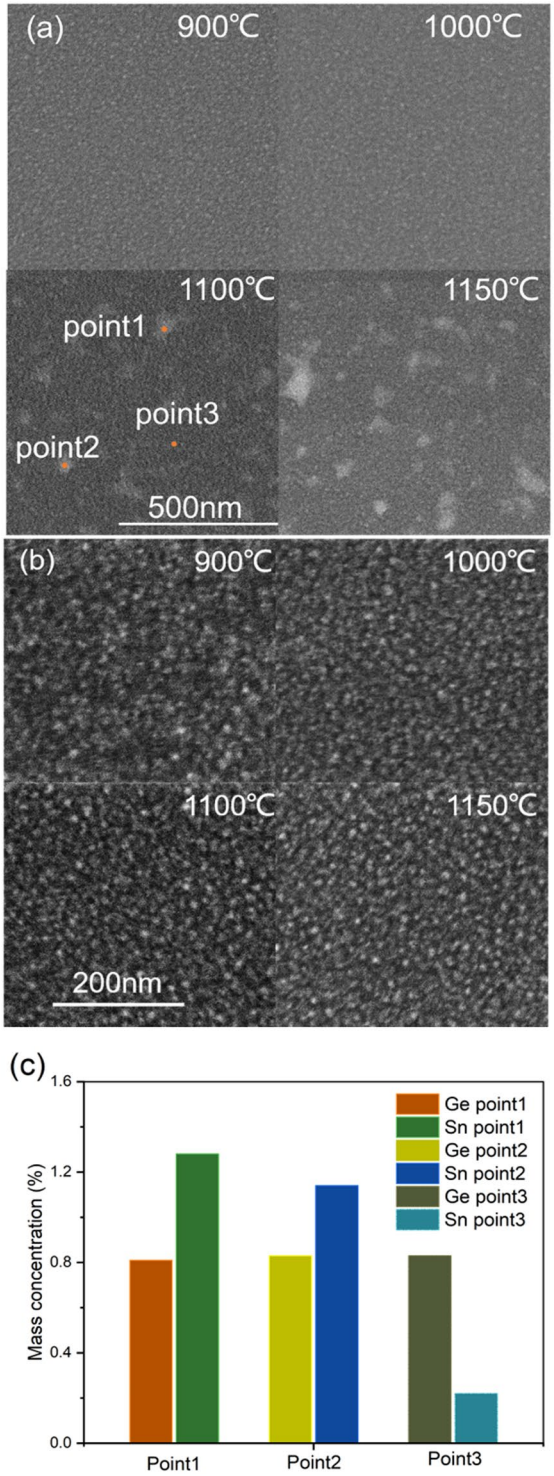

Figure 5. SEM images of (**a**) $Si_{1-x-y}Ge_xSn_y$ and (**b**) $Si_{0.889}Ge_{0.111}$ films after 15 s RTA. (**c**) Mass concentration of Ge and Sn atoms analyzed by EDS at point 1, 2, and point 3 in the $Si_{1-x-y}Ge_xSn_y$ sample after RTA at 1100 °C for 15 seconds.

the highest power factor of the $Si_{0.889}Ge_{0.111}$ sample is one order of magnitude lower than the corresponding $Si_{1-x-y}Ge_xSn_y$ sample, which further proves that the introduction of Sn can greatly improve the thermoelectric property of $Si_{1-x}Ge_x$-based material. In stark contrast to our results, Paul *et al.*[39] prepared nanoporous p-type $Ca_3Co_4O_9$ thin films with a power factor of 2.3 $\mu Wcm^{-1} K^{-2}$ at room temperature, Zhou *et al.*[40] reported a p-type copper telluride nanowires with a power factor of 0.23 $\mu Wcm^{-1} K^{-2}$ at RT, Park *et al.*[41] prepared a p-type RTCVD graphene/PEDOT:PSS (RCG/P) hybrid film which power factor is 0.58 $\mu Wcm^{-1} K^{-2}$ at ~300 K.

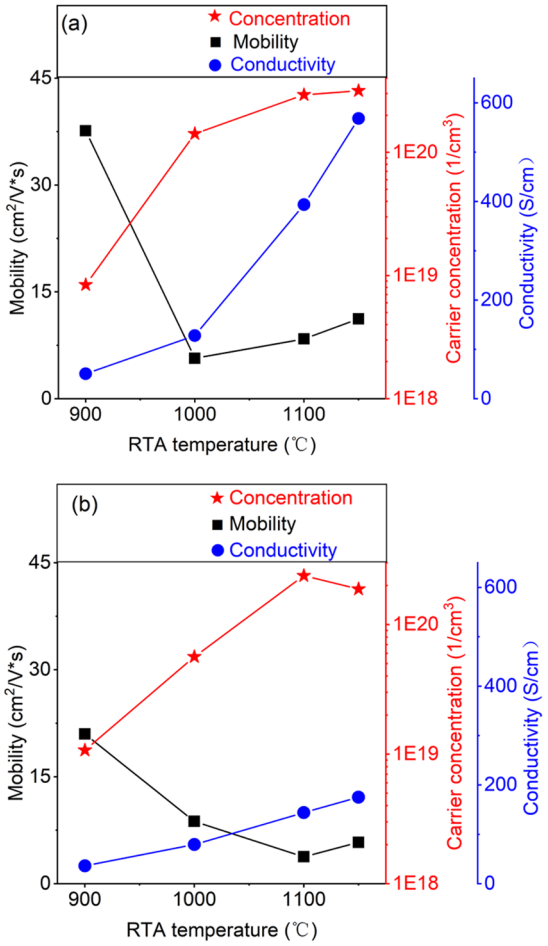

Figure 6. Hall measurement results (mobility, carrier concentration, and conductivity) of (**a**) $Si_{1-x-y}Ge_xSn_y$ and (**b**) $Si_{0.889}Ge_{0.111}$ samples after 15 seconds-RTA as a function of the RTA temperature.

For some references, the thermal conductivity is likely to be even lower than that of $Si_{1-x}Ge_x$ in ternary $Si_{1-x-y}Ge_xSn_y$ alloys with increased mass and bond disorder[17,42], the thermal conductivity is 1.1 W/mK for the sample annealed at 1100 °C for 15 second, matches with the literature[17] value very well. The maximum zT value in this work can reach up to 0.31 at room temperature due to the super low thermal conductivity and the ultrahigh electrical conductivity.

Conclusions

A champion material with key features such as abundance, low toxicity, biocompatibility polycrystalline $Si_{1-x-y}Ge_xSn_y$ films have been successfully deposited on Si/SiO_2 wafers. The synthesized $Si_{1-x-y}Ge_xSn_y$ films have a microcrystalline grain structures ranging in size from 7 nanometers to 24 nanometers. It shows that the introduction of Sn into $Si_{1-x}Ge_x$ can significantly improve the conductivity of $Si_{1-x}Ge_x$ based thermoelectric materials at room temperature while obtaining a relatively high Seebeck coefficient. A high power factor value of 11.3 μW cm^{-1} K^{-2} has been achieved for optimized samples at room temperature, which is 5–50 times larger than TE performances of those reported p-type materials of $Ca_3Co_4O_9$[39], copper telluride nanowires[40], RTCVD graphene/PEDOT:PSS (RCG/P) hybrid film[41] at room temperature. The cost-effective and scalable techniques employed in this research point to future impact of the development of ambient thermoelectric materials both in academia and commercial.

Methods

$Si_{1-x-y}Ge_xSn_y$ film deposition. The $Si_{0.864}Ge_{0.108}Sn_{0.028}$ films were deposited by using a magnetron sputtering apparatus (MB6288, ULVAC Company) on Si/SiO_2 wafers with a 300 nm-thick SiO_2 layer. The base pressure was on the order of 1×10^{-5} Pa and the working pressure of Ar gas in the chamber was on the order of 0.1 Pa. Before the deposition, Si/SiO_2 wafers were ultrasonically cleaned with absolute acetone, ethanol, and deionized water for 5 min in sequence, blow-dried by nitrogen, and then placed into the sample holder. The Si, Ge, and Sn compositions were accurately controlled by optimizing output power parameters of each sputter target. The purities of Si, Ge, and Sn targets were higher than 99.99%. After the deposition of $Si_{1-x-y}Ge_xSn_y$ thin film, a 15 nm-thick SiO_2 layer was then sputtered on the top as a protective layer to avoid the oxidation. The structure of the film is shown in Fig. 8 and all of the sputtering parameters are summarized at the Table. 1 in the Supplementary Section.

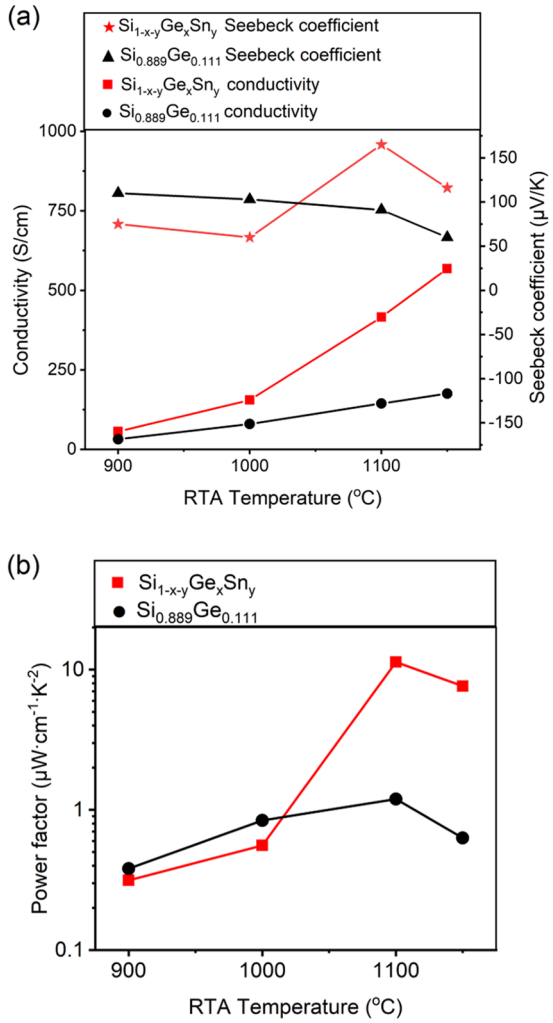

Figure 7. (**a**) The RTA temperature dependence of the Seebeck coefficient and conductivity of samples after 15 seconds-RTA. (**b**) The RTA temperature dependence of the power factor for samples after 15 seconds-RTA.

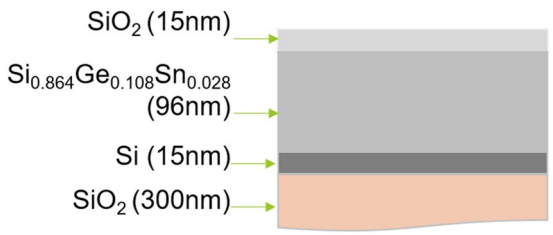

Figure 8. The schematic illustration of the cross-section sample structure.

Ion implantation and RTA process. For improving the thermoelectric properties, the $Si_{0.864}Ge_{0.108}Sn_{0.028}$ layers were implanted with B ion at a dose of 2×10^{15} atoms cm^{-2}. The implantation energy of 16 keV was used to dope into the $Si_{0.864}Ge_{0.108}Sn_{0.028}$ layer. The specific energies and the doses were selected for the ion implantation according to the calculation by using SRIM simulation. The details of the simulation are described in Supplementary Section. Subsequently a 15 seconds short-time RTA in N_2 ambient was performed to electrically activate the dopants in the ternary alloy films, crystallize the $Si_{1-x-y}Ge_xSn_y$ thin film with annihilating defects and achieve a homogeneous doping profile through the whole thickness (AG association Heatpulse 610).

Characterization and thermoelectric performance measurement. The crystal structure and crystallinity of $Si_{1-x-y}Ge_xSn_y$ layer were characterized using the X-ray diffraction (XRD) measurement (Rigaku RINT-2100) with Cu $K_{\alpha 1}$ radiation with a wavelength of 1.54056 Å. The diffraction profiles were measured at a diffraction angle (2θ) from 20° to 65° with in a step of 0.02°. Micro Raman spectroscopy measurement was carried

out using an excitation wavelength of 532 nm and a total laser power of 1.4 mW at room temperature (Nano photon Raman-11). Scanning electron microscopy (SEM Hitachi S-5200) was carried out at an acceleration voltage of 30 kV and a working current of 10 μA. The Hall mobility μ_H and carrier concentration n were measured using a Hall effect measurement system (Toyo corporation RESITEST 8300) at room temperature. The samples used for the measurement were cut into rectangular bars with approximate dimensions about of $1 \times 1\,cm^2$. Conductivity and Seebeck coefficient of samples were measured by using the SBA485 system (Netzsch), and the system errors were below about 7% and the measure temperature was at room temperature. The thermal conductivity of samples were measured using the ultrafast laserbased time-domain thermoreflectance (TDTR) method (Picotherm).

References

1. Morata, A. *et al.* Large-area and adaptable electrospun silicon-based thermoelectric nanomaterials with high energy conversion efficiencies. *Nature Communications* **9**, 4759 (2018).
2. Francioso, L. *et al.* Flexible thermoelectric generator for ambient assisted living wearable biometric sensors. *Journal of Power Sources* **196**, 3239–3243 (2011).
3. Park, H. *et al.* Enhanced thermoelectric properties of PEDOT:PSS nanofilms by a chemical dedoping process. *J. Mater. Chem. A* **2**, 6532–6539 (2014).
4. Park, T., Park, C., Kim, B., Shin, H. & Kim, E. Flexible PEDOT electrodes with large thermoelectric power factors to generate electricity by the touch of fingertips. *Energy & Environmental Science* **6**, 788 (2013).
5. Fan, Z., Li, P., Du, D. & Ouyang, J. Significantly Enhanced Thermoelectric Properties of PEDOT:PSS Films through Sequential Post-Treatments with Common Acids and Bases. *Advanced Energy. Materials* **7**, 1602116 (2017).
6. Culebras, M. *et al.* Manufacturing Te/PEDOT Films for Thermoelectric Applications. *ACS Applied Materials & Interfaces* **9**, 20826–20832 (2017).
7. Bae, E. J., Kang, Y. H., Lee, C. & Cho, S. Y. Engineered nanocarbon mixing for enhancing the thermoelectric properties of a telluride-PEDOT:PSS nanocomposite. *Journal of Materials Chemistry A* **5**, 17867–17873 (2017).
8. Culebras, M. *et al.* High Thermoelectric Power Factor Organic Thin Films through Combination of Nanotube Multilayer Assembly and Electrochemical Polymerization. *ACS Applied Materials & Interfaces* **9**, 6306–6313 (2017).
9. Sun, Y. *et al.* Flexible n-Type High-Performance Thermoelectric Thin Films of Poly(nickel-ethylenetetrathiolate) Prepared by an Electrochemical Method. *Advanced Materials* **28**, 3351–3358 (2016).
10. Haras, M. *et al.* Fabrication of Thin-Film Silicon Membranes With Phononic Crystals for Thermal Conductivity Measurements. *IEEE Electron Device Letters* **37**, 1358–1361 (2016).
11. LeBlanc, S., Yee, S. K., Scullin, M. L., Dames, C. & Goodson, K. E. Material and manufacturing cost considerations for thermoelectrics. *Renewable and Sustainable Energy Reviews* **32**, 313–327 (2014).
12. Bhandari, C. M. & Rowe, D. M. CRC Handbook of thermoelectrics. *CRC Press, Boca Raton, FL* **49** (1995).
13. Pei, Y. *et al.* Convergence of electronic bands for high performance bulk thermoelectrics. *Nature* **473**, 66–69 (2011).
14. Zhao, W. *et al.* Superparamagnetic enhancement of thermoelectric performance. *Nature* **549**, 247–251 (2017).
15. Hicks, L. D. & Dresselhaus, M. S. Effect of quantum-well structures on the thermoelectric figure of merit. *Physical Review B* **47**, 12727–12731 (1993).
16. Kurosawa, M. *et al. (Invited)* A New Application of $Ge_{1-x}Sn_x$: Thermoelectric Materials. *ECS Transactions* **86**, 321–328 (2018).
17. Khatami, S. N. & Aksamija, Z. Lattice Thermal Conductivity of the Binary and Ternary Group-IV Alloys Si-Sn, Ge-Sn, and Si-Ge-Sn. *Physical Review Applied* **6** (2016).
18. Moontragoon, P., Soref, R. A. & Ikonic, Z. The direct and indirect bandgaps of unstrained $Si_xGe_{1-x-y}Sn_y$ and their photonic device applications. *Journal of Applied Physics* **112**, 073106 (2012).
19. Gaiduk, P. I., Lundsgaard Hansen, J., Nylandsted Larsen, A., Bregolin, F. L. & Skorupa, W. Suppression of tin precipitation in SiSn alloy layers by implanted carbon. *Applied Physics Letters* **104**, 231903 (2014).
20. German, R. M. Intermediate Stage Processes: Solution-Reprecipitation. In *Liquid Phase Sintering* 101–126 (Springer US), https://doi.org/10.1007/978-1-4899-3599-1_5 (1985).
21. Renucci, J. B., Renucci, M. A. & Cardona, M. Volume dependence of the Raman frequencies of Ge Si alloys. *Solid State Communications* **9**, 1651–1654 (1971).
22. Brya, W. J. Raman scattering in Ge Si alloys. *Solid State Communications* **12**, 253–257 (1973).
23. D'Costa, V. R., Tolle, J., Poweleit, C. D., Kouvetakis, J. & Menéndez, J. Compositional dependence of Raman frequencies in ternary $Ge_{1-x-y}Si_xSn_y$ alloys. *Physical Review B* **76** (2007).
24. Liu, J. *et al.* The effects of ZnO layer and annealing temperature on the structure, optical and film–substrate cohesion properties of SiGe thin films prepared by radio frequency magnetron sputtering. *Applied Surface Science* **259**, 393–398 (2012).
25. Monshi, A., Foroughi, M. R. & Monshi, M. R. Modified Scherrer Equation to Estimate More Accurately Nano-Crystallite Size Using XRD. *World Journal of Nano Science and Engineering* **02**, 154–160 (2012).
26. Kacher, J., Landon, C., Adams, B. L. & Fullwood, D. Bragg's Law diffraction simulations for electron backscatter diffraction analysis. *Ultramicroscopy* **109**, 1148–1156 (2009).
27. Teh, L. K., Choi, W. K., Bera, L. K. & Chim, W. K. Structural characterisation of polycrystalline SiGe thin film. *Solid-State Electronics* **45**, 1963–1966 (2001).
28. Li, V. Z.-Q. *et al.* Structure and properties of rapid thermal chemical vapor deposited polycrystalline silicon–germanium films on SiO2 using Si2H6, GeH4, and B2H6 gases. *Journal of Applied Physics* **83**, 5469–5476 (1998).
29. Lu, J., Guo, R., Dai, W. & Huang, B. Enhanced in-plane thermoelectric figure of merit in p-type SiGe thin films by nanograin boundaries. *Nanoscale* **7**, 7331–7339 (2015).
30. Neophytou, N. *et al.* Simultaneous increase in electrical conductivity and Seebeck coefficient in highly boron-doped nanocrystalline Si. *Nanotechnology* **24**, 205402 (2013).
31. Stöckhert, B. & Duyster, J. Discontinuous grain growth in recrystallised vein quartz — implications for grain boundary structure, grain boundary mobility, crystallographic preferred orientation, and stress history - ScienceDirect. *Journal of Structural Geology* **21**, 1477–1490 (1999).
32. Ukawa, K. *et al.* Activation of Silicon Implanted with Phosphorus and Boron Atoms by Infrared Semiconductor Laser Rapid Annealing. *Japanese Journal of Applied Physics* **49**, 076503 (2010).
33. Liufu, S.-C., Chen, L.-D., Yao, Q. & Wang, C.-F. Assembly of one-dimensional nanorods into Bi2S3 films with enhanced thermoelectric transport properties. *Applied Physics Letters* **90**, 112106 (2007).
34. Makala, R. S., Jagannadham, K. & Sales, B. C. Pulsed laser deposition of Bi2Te3-based thermoelectric thin films. *Journal of Applied Physics* **94**, 3907–3918 (2003).
35. Yao, Q., Chen, L., Xu, X. & Wang, C. The High Thermoelectric Properties of Conducting Polyaniline with Special Submicron-fibre Structure. *Chemistry Letters* **34**, 522–523 (2005).
36. Raz, T., Edelman, F., Komem, Y., Stölzer, M. & Zaumseil, P. Transport properties of boron-doped crystallized amorphous $Si_{1-x}Ge_x$ films. *Journal of Applied Physics* **84**, 4343–4350 (1998).

37. Vining, C. B., Laskow, W., Hanson, J. O., Van der Beck, R. R. & Gorsuch, P. D. Thermoelectric properties of pressure-sintered Si0.8Ge0.2 thermoelectric alloys. *Journal of Applied Physics* **69**, 4333–4340 (1991).
38. Dismukes, J. P., Ekstrom, L., Steigmeier, E. F., Kudman, I. & Beers, D. S. Thermal and Electrical Properties of Heavily Doped Ge-Si Alloys up to 1300°K. *Journal of Applied Physics* **35**, 2899–2907 (1964).
39. Paul, B., Björk, E. M., Kumar, A., Lu, J. & Eklund, P. Nanoporous $Ca_3Co_4O_9$ Thin Films for Transferable Thermoelectrics. *ACS Applied Energy Materials* **1**, 2261–2268 (2018).
40. Zhou, C. *et al*. Nanowires as Building Blocks to Fabricate Flexible Thermoelectric Fabric: The Case of Copper Telluride Nanowires. *ACS Applied Materials & Interfaces* **7**, 21015–21020 (2015).
41. Park, C. *et al*. Large-scalable RTCVD Graphene/PEDOT:PSS hybrid conductive film for application in transparent and flexible thermoelectric nanogenerators. *RSC Advances* **7**, 25237–25243 (2017).
42. Kouvetakis, J., Menendez, J. & Tolle, J. Advanced Si-based Semiconductors for Energy and Photonic Applications. *Solid State Phenomena* **156–158**, 77–84 (2009).

Acknowledgements

This work was partly supported by PRESTO (Grant No. JPMJPR15R2) and CREST (Grant No. JPMJCR19Q5) from the JST in Japan, a research grant (Creation of Life Innovation Materials for Interdisciplinary and International Researcher Development) from the MEXT in Japan, the National Natural Science Foundation of China (Grant Nos 51572049 and 51602068), and the Guangxi Natural Science Foundation of China (Grant No. 2015GXNSFFA139002). Thanks for the thermal conductivity measurement and discussion from Prof. Tsunehiro Takeuchi in Toyota Technological Institute, Japan.

Author Contributions

Y.P. designed the experiment and performed most of the fabrication of thermoelectric $Si_{1-x-y}Ge_xSn_y$ films and manuscript preparation. L.M. contributed significantly to manuscript preparation. O.N. contributed to the analysis of XRD, SEM characterization and manuscript promotion. Y.P. prepared the manuscript with discussion from J.G., C.Y.L, M.K. and S.Z. All the authors discussed the results.

Additional Information

Supplementary information accompanies this paper at https://doi.org/10.1038/s41598-019-50754-4.

Competing Interests: The authors declare no competing interests.

Publisher's note Springer Nature remains neutral with regard to jurisdictional claims in published maps and institutional affiliations.